Research article

NMR IN BIOMEDICINE

Received: 7 May 2014, Revised: 10 November 2014, Accepted: 19 December 2014, Published online in Wiley Online Library

(wileyonlinelibrary.com) DOI: 10.1002/nbm.3259

In vivo visualization and *ex vivo* quantification of murine breast cancer cells in the mouse brain using MRI cell tracking and electron paramagnetic resonance

Pierre Danhier[a], Julie Magat[a], Philippe Levêque[a], Géraldine De Preter[a], Paolo E. Porporato[b], Caroline Bouzin[b], Bénédicte F. Jordan[a], Gladys Demeur[c], Vincent Haufroid[c], Olivier Feron[b], Pierre Sonveaux[b] and Bernard Gallez[a]*

Cell tracking could be useful to elucidate fundamental processes of cancer biology such as metastasis. The aim of this study was to visualize, using MRI, and to quantify, using electron paramagnetic resonance (EPR), the entrapment of murine breast cancer cells labeled with superparamagnetic iron oxide particles (SPIOs) in the mouse brain after intracardiac injection.

For this purpose, luciferase-expressing murine 4 T1-luc breast cancer cells were labeled with fluorescent Molday ION Rhodamine B SPIOs. Following intracardiac injection, SPIO-labeled 4 T1-luc cells were imaged using multiple gradient-echo sequences. *Ex vivo* iron oxide quantification in the mouse brain was performed using EPR (9 GHz). The long-term fate of 4 T1-luc cells after injection was characterized using bioluminescence imaging (BLI), brain MRI and immunofluorescence.

We observed hypointense spots due to SPIO-labeled cells in the mouse brain 4 h after injection on T_2*-weighted images. Histology studies showed that SPIO-labeled cancer cells were localized within blood vessels shortly after delivery. *Ex vivo* quantification of SPIOs showed that less than 1% of the injected cells were taken up by the mouse brain after injection. MRI experiments did not reveal the development of macrometastases in the mouse brain several days after injection, but immunofluorescence studies demonstrated that these cells found in the brain established micrometastases. Concerning the metastatic patterns of 4 T1-luc cells, an EPR biodistribution study demonstrated that SPIO-labeled 4 T1-luc cells were also entrapped in the lungs of mice after intracardiac injection. BLI performed 6 days after injection of 4 T1-luc cells showed that this cell line formed macrometastases in the lungs and in the bones.

Conclusively, EPR and MRI were found to be complementary for cell tracking applications. MRI cell tracking at 11.7 T allowed sensitive detection of isolated SPIO-labeled cells in the mouse brain, whereas EPR allowed the assessment of the number of SPIO-labeled cells in organs shortly after injection.

Keywords: electron paramagnetic resonance; MRI; cell tracking; cancer; metastasis; iron oxide particles

INTRODUCTION

It is necessary to monitor the fate of cells of interest after injection for the successful application of cell-based therapies and the understanding of fundamental processes of cancer biology (e.g. metastasis) (1). *In vivo* MRI cell tracking of magnetically labeled cells has been extensively developed for such applications. Although MR reporter genes such as ferritin have been used for tracking cells (2–4), superparamagnetic iron oxide particles (SPIOs) are more widely used as labeling contrast agents because they induce signal voids on T_2- and T_2*-weighted images

* *Correspondence to: Bernard Gallez, Louvain Drug Research Institute, Biomedical Magnetic Resonance Research Group, Université catholique de Louvain, Brussels, Belgium. E-mail: bernard.gallez@uclouvain.be*

a *P. Danhier, J. Magat, P. Levêque, G. De Preter, B. F. Jordan, B. Gallez*
Louvain Drug Research Institute, Biomedical Magnetic Resonance Research Group, Université catholique de Louvain, Brussels, Belgium

b *P. E. Porporato, C. Bouzin, O. Feron, P. Sonveaux*
Institut de Recherche Expérimentale et Clinique (IREC), Pole of Pharmacology, Université catholique de Louvain, Brussels, Belgium

c *G. Demeur, V. Haufroid*
Louvain Center for Toxicology and Applied Pharmacology, Université catholique de Louvain, Brussels, Belgium

Abbreviations used: *BLI, bioluminescence imaging; CTC, circulating tumor cell; EPR, electron paramagnetic resonance; ICP-MS, inductively coupled plasma mass spectroscopy; LOD, limit of detection; LOQ, limit of quantification; MGE, multiple gradient-echo; MIRB, Molday ION Rhodamine B; PBS, phosphate-buffered saline; RARE, rapid acquisition with relaxation enhancement; ROI, region of interest; SEM, standard error of the mean; SNR, signal-to-noise ratio; SP, superparamagnetic; SPIO, superparamagnetic iron oxide particles; T_2-w, T_2 weighted; T_2*-w, T_2* weighted.*

and are biocompatible (5). Although developments have led to single-cell detection (6,7), quantitative methods are nevertheless needed to accurately assess the distribution of labeled cells in living organisms. Non-invasive quantification methods mostly rely on relaxometry-based techniques or retrieval of information on magnetic field inhomogeneities from phase maps (8). Relaxometry-based techniques are not directly applicable *in vivo* because physiological processes such as SPIO compartmentalization, cell division and particle release from cells affect the relaxation properties of SPIOs (9,10). Furthermore, Rad *et al*. have shown that different cell lines labeled with the same type of particle and having comparable intracellular iron oxide contents exhibit different relaxation rates (11). A recent method based on modeling the magnetic field inhomogeneities induced by SPIO showed accurate estimates of iron oxide content in phantoms and *in vivo*. However, this model was sensitive to tissue–tissue and air–tissue interfaces and assumed that the SPIO distribution was homogenous in the region of interest (ROI) (8).

Non-invasive quantification of SPIOs for cell tracking applications remains challenging because the presence of endogenous iron, SPIOs released from labeled cells, and clustering and distribution of SPIOs within the tissue are factors that strongly influence the relaxation properties of iron oxides (8,12). To our knowledge, successful *in vivo* quantification has been reported in one study after intra-articular administration of bone-marrow-derived mesenchymal stem cells labeled with SPIOs (13). In this study, cells were localized in a confined space and their exact number was known. On the other hand, electron paramagnetic resonance (EPR) spectroscopy has been shown in several studies to be a robust method for assessing the fate of SPIOs after administration in living animals (14,15). As a consequence, the quantitative information provided by the EPR method might be useful for the development of new *in vivo* methods for SPIO quantification.

In the present study, using high field MRI (11.7 T), we aimed to track the settling into the mouse brain of luciferase-expressing 4 T1-luc breast cancer cells labeled with Molday ION Rhodamine B (MIRB) SPIOs initially injected into the heart. 4 T1 cells have been described as establishing brain metastases after intracardiac injection (16,17). MIRB iron oxide nanoparticles (colloidal size of 35 nm) have been previously shown to be nontoxic and to be retained within the cell cytoplasm after labeling (18,19). In this study, the iron oxide content in the brain was assessed *ex vivo* using EPR. Although animal sacrifice is required, this technique was used in several studies for absolute SPIO quantification after injection (14,15,20–24). EPR spectroscopy at room temperature allows the specific measurement of the SPIOs without interference by endogenous iron (14,15). Using both MRI for SPIO-labeled cell visualization and EPR for SPIO quantification, we wanted to assess the complementarity of the two methods for cell tracking studies.

EXPERIMENT

Ethical statement

All *in vivo* experiments were performed in compliance with guidelines set by national regulations and were approved by the ethical committee for animal care of the Université catholique de Louvain.

MRI

In vivo MR experiments on mouse brains were performed with an 11.7 T system (Bruker, Ettlingen, Germany) equipped with a cryoprobe. Animals were anesthetized by inhalation of 1.5–2% isoflurane (Forene, Abbott, Maidenhead, UK). Mouse temperature was maintained at 37.0 °C and respiration was monitored. coronal T_2-weighted (T_2-w) images were acquired using a turbo rapid acquisition with relaxation enhancement (RARE) sequence with the following parameters: T_R, 2500 ms; T_E, 39.1 ms; refocusing flip angle, 180°; RARE factor, 8; field of view, 2 cm × 2 cm; matrix, 350 × 350; slice thickness, 1 mm; number of slices, 10; in-plane resolution, 57 μm × 57 μm. Coronal T_2*-weighted (T_2*-w) images were acquired using a multiple gradient-echo (MGE) sequence with the following parameters: T_R, 2000 ms; T_E, 5 ms; excitation pulse angle, 30°; field of view, 2 cm × 2 cm; matrix, 350 × 350; slice thickness, 1 mm; number of slices, 10; in-plane resolution, 57 μm × 57 μm. For visualizing SPIO-labeled murine breast cancer 4 T1-luc cells in the mouse brain, animals ($n = 3$) were scanned using T_2-, T_2*-w images 4 h after injection (day 0) and 1, 2 and 3 days post-injection of 10^6 MIRB-labeled 4 T1-luc cells. The same mice underwent bioluminescence imaging (BLI) at day 6 post-injection and MRI scans (T_2-w images) 13 days post-injection for monitoring the development of cerebral metastases, and were next sacrificed. The presence of 4 T1 metastases in the brain was then characterized using histology.

In vitro MRI was also performed on 4% gelatin phantoms containing 3×10^5 living cells/mL using MGE sequences with the same parameters as used for *in vivo* imaging (25). Signal-to-noise ratios (SNRs) of phantom images were determined by dividing the mean intensity value of an ROI, drawn using ImageJ software (NIH), by the standard deviation of the same ROI.

Ex vivo endogenous iron and exogenous iron oxide determination

Mice injected in the left ventricle with 10^6 MIRB-labeled 4 T1-luc cells or free MIRB nanoparticles (5 μg Fe) as a control were sacrificed after MRI examination. Iron oxide content in the brains, livers, spleens, lungs, hearts and kidneys of mice was determined *ex vivo* using X-band EPR (9 GHz). After animal sacrifice, organs were harvested, freeze-dried and crushed into a fine powder. Dry samples were then weighed and analyzed using EPR with the following settings: microwave power, 5.05 mW; center field, 3150 G; field sweep width, 5000 G; modulation amplitude, 30 G; time constant, 20.48 ms; conversion time, 20.48 ms; modulation field, 100 kHz. Measurements were made at room temperature. The iron oxide content in each freeze-dried organ was quantified by comparison with a calibration curve of dry MIRB standards. The limit of detection (LOD) and quantification (LOQ) were assessed using a calibration curve for different concentrations of MIRB-labeled cells after water removal (oven at 60 °C for 3 days). They were calculated using the formulas LOD = 3 SD/a and LOQ = 10 SD/a (SD, standard deviation of the intercept; a, slope of the calibration curve). Endogenous iron content was also determined in whole dry organs of mice that did not receive SPIO injection using inductively coupled plasma mass spectroscopy (ICP-MS).

Statistical analyses

All results are represented as means ± standard error of the mean (SEM). Comparisons between groups were performed using

NMR IN BIOMEDICINE

Student's *t*-test; $p < 0.05$ was considered to be statistically significant.

Supplementary methods

Protocols for cell labeling, intracellular SPIO quantification, intracardiac injection, Prussian blue staining, BLI and immunohistochemistry are detailed in the supplementary data section.

RESULTS

EPR quantification of MIRB cell labeling

Fluorescence microscopy images (Fig. 1(A)) showed that 4 T1 cells efficiently internalized fluorescent MIRB particles. SPIOs were localized within the cytoplasm after incubation. After labeling, 4.62 ± 0.26 pg superparamagnetic (SP) Fe was internalized per cell ($n = 3$). Calibration curves recorded with increasing concentrations of water-free MIRB-labeled cells showed that EPR could detect 2100 MIRB-labeled cells and that the LOQ was equal to 7200 MIRB-labeled cells (Fig. 1(B)).

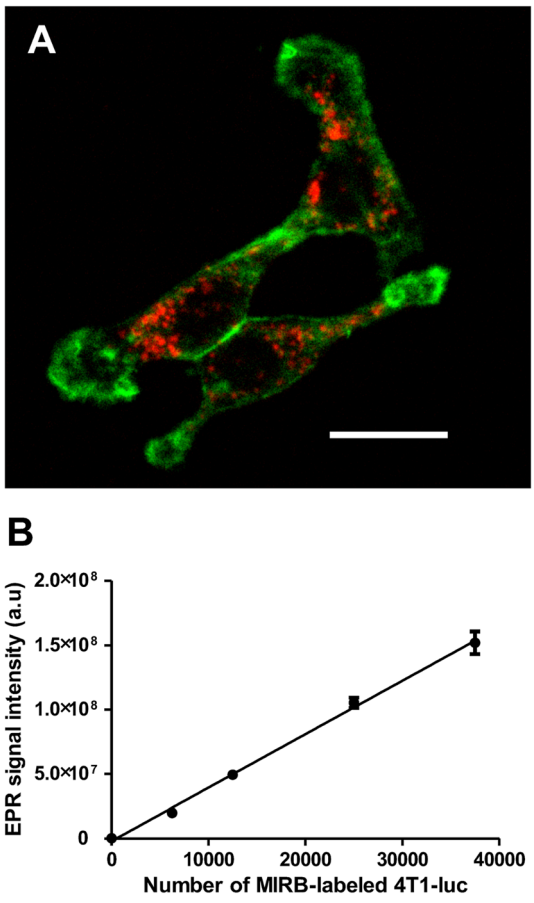

Figure 1. EPR detection of 4 T1-luc cells labeled with MIRB nanoparticles. (A) Fluorescence microscopy of 4 T1-luc cells labeled with MIRB (red fluorescence). Actin is stained in green using phalloidin-FITC. The scale bar represents 20 μm. (B) Linear regression of increasing numbers of MIRB-labeled cells after water removal using X-band EPR ($n = 4$). Data are expressed as mean ± SEM.

MRI can detect isolated SPIO-labeled tumor cells in the mouse brain

In vivo MRI was performed to monitor the fate of MIRB-labeled 4 T1-luc cells in the mouse brain after intracardiac injection ($n = 3$). As shown in Fig. 2(A), numerous hypointense spots were observed on T_2*-w images 4 h after injection of 10^6 MIRB-labeled cells, whereas anatomical T_2-w images did not display these features. Hypointense spots decreased with time and became undetectable 3 days post-injection (Fig. 2(B)). In a control experiment, T_2*-w images of gelatin phantoms containing MIRB-labeled cells (3×10^5 cells/mL) showed numerous signal voids ($n = 3$), whereas unlabeled 4 T1 cells ($n = 3$) at the same concentration did not induce negative contrast on MR images (Fig. 3). As shown in Figure 3(B), a drop in SNR values was observed in the 4 T1 + MIRB group compared with unlabeled cells (6.73 ± 0.10 for 4 T1 + MIRB versus 8.49 ± 0.33 for unlabeled 4 T1 cells). The Prussian blue staining performed after brain imaging on day 0 confirmed the presence of iron-positive cells (Fig. 4). Interestingly, only isolated or small clusters of Prussian blue-positive cells were found within brain blood vessels, highlighted using periodic acid–Schiff counterstaining.

After intracardiac injection, mouse brain and lungs trap MIRB-labeled 4 T1 tumor cells preferentially to cell-free MIRB particles

Having visualized isolated MIRB-labeled 4 T1-luc cells using MRI at 11.7 T, we next wanted to know how many SPIO-labeled cancer cells were entrapped in the mouse brain after intracardiac injection. Figure 5(A) shows that hypointense spots were detected on T_2*-w images 4 h after injection of 10^6 MIRB-labeled cells ($n = 3$), whereas no negative contrast was observed when mice received free MIRB particles (corresponding to 5 μg SP Fe) ($n = 3$). This dose corresponded to the iron content of 10^6 MIRB-labeled cells. After MR imaging, iron oxide content of brain, liver, spleen, lungs, heart and kidneys was assessed using *ex vivo* EPR. Significant levels of SPIO were found in the brains of mice injected with SPIO-labeled 4 T1 cells, whereas a negligible EPR signal was detected in the brains of control mice (Fig. 5(B), 0.52 ± 0.11 ng SP Fe/mg brain tissue for the 4 T1 + MIRB group

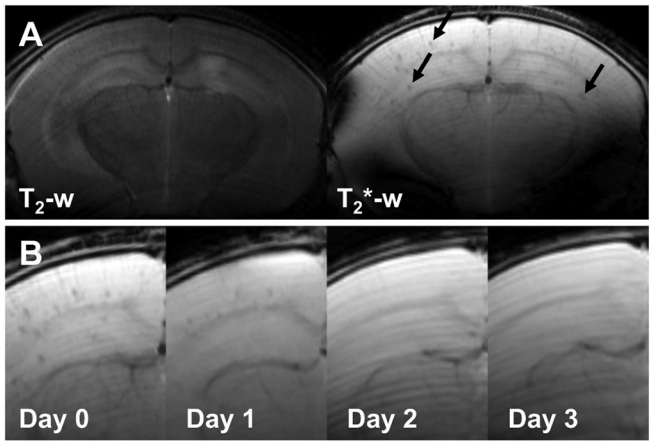

Figure 2. MR visualization of MIRB-labeled 4 T1-luc cells 4 h after intracardiac injection. (A) Signal voids (black arrows) were detected on T_2*-w images 4 h after injection of 10^6 MIRB-labeled 4 T1-luc cells, whereas no hypointensities were observed on T_2-w images ($n = 3$). (B) A progressive loss of signal voids was observed in the days after injection.

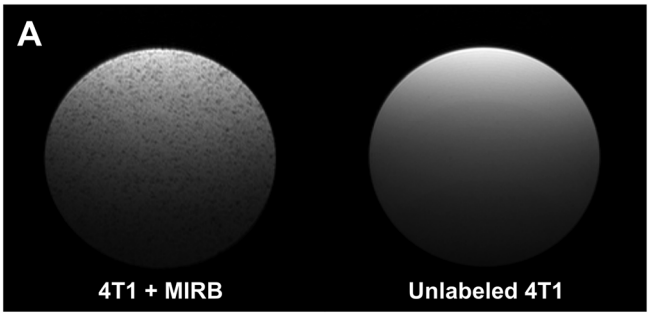

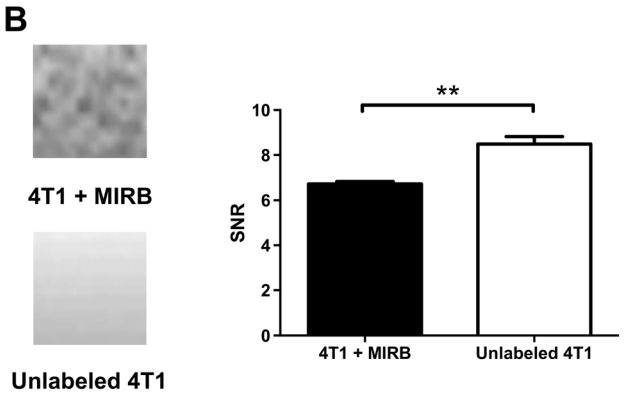

Figure 3. MR phantom images of MIRB-labeled 4 T1-luc. (A) T_2*-w images of gelatin (4%) phantoms containing MIRB-labeled 4 T1-luc cells or unlabeled cells showed that signal voids were due to MIRB-labeled cells ($n = 3$). (B) Magnification and SNR values of MR phantom images ($n = 3$). Data are expressed as mean ± SEM. $^{**}p < 0.01$.

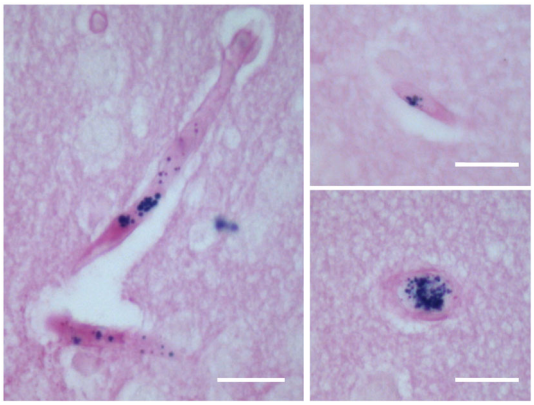

Figure 4. Histological confirmation of the presence of iron oxides in mouse brains after MRI. Prussian blue staining confirmed the presence of isolated iron-positive cells in the mouse brain 4 h after intracardiac injection of MIRB-labeled 4 T1-luc cells. Periodic acid–Schiff counterstaining showed that single iron-positive cells or small clusters of cells were localized within blood vessels. The scale bar represents 20 μm.

versus 0.01 ± 0.00 ng SP Fe/mg tissue for the MIRB group). Detected levels of SP iron were much lower (<3%) than endogenous brain iron levels (Table 1, 23.05 ± 1.28 ng Fe/mg tissue). One day post-injection, the iron oxide content dropped in the brain (Fig. 5(C)) and a statistical difference between groups ($n = 4$ for each group) was no longer observed (0.14 ± 0.07 ng SP Fe/mg tissue for the 4 T1 + MIRB group versus 0.02 ± 0.01 ng SP Fe/mg tissue for the MIRB group). As shown in Fig. 6, significantly higher iron oxide levels were also found in the lungs of mice injected with MIRB-labeled 4 T1-luc cells in comparison with the MIRB group at day 0 (28.59 ± 3.03 ng SP Fe/mg tissue for the 4 T1 + MIRB group versus 0.38 ± 0.12 46 ng SP Fe/mg tissue for the MIRB group). Typical EPR spectra of brain and lung samples are shown in Fig. 7(A) and (B), respectively. The sharp EPR line observed in EPR spectra (Fig. 7(A)) has been reported in other studies and was attributed to the presence of free radicals (15,26). Of note, this sharp EPR spectrum had a negligible contribution to the broad EPR signal arising from iron oxides (15).

Iron oxide content in other organs was also measured (Fig. 6). Four hours after intracardiac injection, iron oxide levels in the liver were 3.83 ± 0.57 ng SP Fe/mg tissue for the 4 T1 + MIRB group and 8.65 ± 1.21 ng SP Fe/mg tissue for mice that received free MIRB, showing that the liver initially preferentially captures free particles. Similarly, higher iron oxide levels were found in the spleens of mice injected with free SPIO in comparison with the 4 T1 + MIRB group (Fig. 6, 8.59 ± 1.55 ng SP Fe/mg tissue for the 4 T1 + MIRB group versus 43.06 ± 1.46 ng SP Fe/mg tissue for the MIRB group). No statistical difference was observed in SPIO content in the kidneys for the two groups (0.98 ± 0.39 ng SP Fe/mg tissue for the 4 T1 + MIRB group versus 0.81 ± 0.32 ng SP Fe/mg tissue for the MIRB group at day 0). Although no statistical difference was found, SPIO levels tended to be higher in hearts injected with MIRB-labeled 4 T1-luc compared with hearts receiving free SPIOs (Fig. 6, 29.36 ± 19.32 ng SP Fe/mg tissue for the 4 T1 + MIRB group versus 0.61 ± 0.05 ng SP Fe/mg tissue for the MIRB group at day 0). As also shown in Fig. 6, iron oxide levels in all tissues dropped in both treatment groups one day after injection. Basal endogenous iron levels measured using ICP-MS in different organs ($n = 5$) were much more important than the levels of SPIOs detected in tissues (Table 1). For instance, 23.05 ± 1.28 ng endogenous Fe/mg tissue was measured in brains of control mice.

Long-term assessment of the fate of SPIO-labeled murine breast cancer cells in the brain

After visualizing *in vivo* and quantifying *ex vivo* the number of SPIO-labeled 4 T1 cells localized in the brain, we addressed the question of whether a subset of these entrapped cancer cells could establish successful metastases. Using BLI ($n = 3$), 4 T1-luc cells were shown to develop large metastases in lungs and bones 6 days after intracardiac injection (Fig. 8). BLI-positive spots were also observed at the injection site (heart). No bioluminescence was detected in the brain of these mice. However, mice showed severe signs of weakness 13 days after intracardiac injection, and mouse brains were therefore scanned using MRI to detect brain metastases. Figure 9(A) shows that no macrometastases were detected on conventional T_2-w images. Immunofluorescence images (Fig. 9(B)) nevertheless demonstrated the invasion of the brain parenchyma by numerous luciferase-positive brain micrometastases (~100 μm).

DISCUSSION

Using MRI and *ex vivo* EPR, we succeeded in visualizing and quantifying SPIO in circulating tumor cells (CTCs) entrapped in the mouse brain after intracardiac injection. As demonstrated with phantom studies, isolated cells and small clusters of SPIO-labeled cells were detected, whereas unlabeled cells could not be visualized on T_2*-w images. Nevertheless, MR images showed

NMR IN BIOMEDICINE

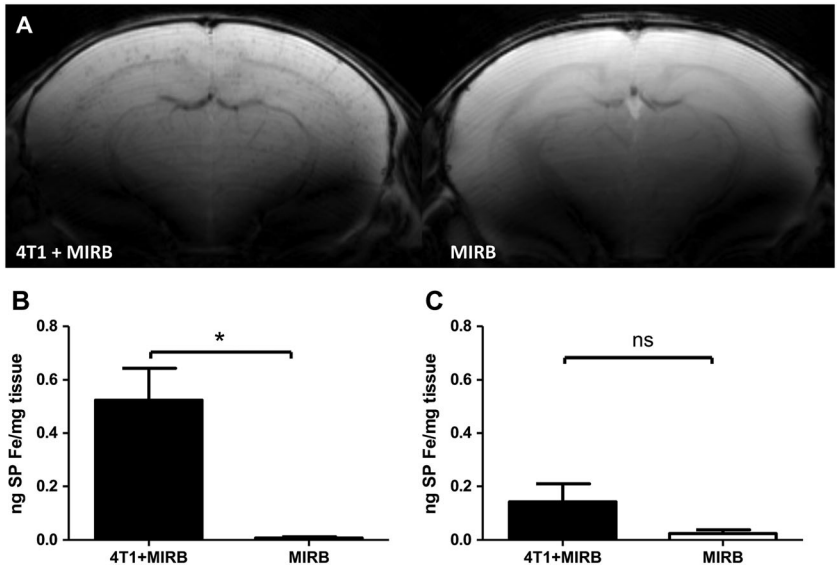

Figure 5. Correlation between MR detection of MIRB-labeled 4 T1-luc cells and *ex vivo* EPR quantification of iron oxides in mouse brains. (A) MR images produced 4 h after administration of 10^6 MIRB-labeled cells or 5 μg SP Fe of free MIRB particles. No signal voids were detected in mice receiving free MIRB ($n = 3$). (B) After MRI, a major difference in iron oxide content in the brain was found between mice injected with MIRB-labeled cells and mice injected with free MIRB 4 h post-injection ($n = 3$). (C) Brain iron oxide levels dropped one day post-injection and no statistical difference was found between the 4 T1-luc + MIRB group and free MIRB group ($n = 4$). Data are expressed as mean ± SEM. *$p < 0.05$; ns, $p > 0.05$.

Table 1. Endogenous iron levels in organs of BALB/c mice (mean ± SEM, $n = 5$)

Organ	Endogenous iron (ng Fe/mg tissue)
Brain	23.05 ± 1.28
Liver	165.99 ± 5.09
Spleen	457.88 ± 18.73
Lungs	160.01 ± 8.65
Heart	181.25 ± 27.79
Kidneys	89.62 ± 9.15

that signal voids due to SPIO-labeled cells decreased in the days post-injection. This can be explained by the dilution of the intracellular SPIO content with cell proliferation (27), SPIO metabolism (28,29) and the clearance of SPIO released by dead cells from the brain (30). It was also shown using EPR that the iron oxide content in the mouse brain dropped below the detection threshold one day post-injection. As the dilution of SPIOs due to cell proliferation should not affect the total iron oxide content in the brain, this decrease is likely essentially due to the clearance and degradation of SPIOs. Indeed, it was shown that the dextran coating of SPIOs is degraded in lysosomal environments (29). Therefore, the iron oxide core can be dissolved at acidic pH in the presence of metallic chelates (29). Labeling cancer cells with micron-sized iron oxides coated with an inert styrene/divinylbenzene layer could circumvent this possible drawback. However, MIRB nanoparticles were preferred owing to their excellent labeling properties (18,24,31) and their biocompatibility (19,32). As EPR measurements made at room temperature are specific for SPIOs (14,15), we used ICP-MS as an alternative quantification method for measuring total iron content in tissues. Basal endogenous iron levels were found to be high in mouse tissues (ranging from ~25 ng Fe/mg tissue for the mouse brain to ~460 ng Fe/mg tissue for the spleen) compared with iron oxide levels found in these tissues after cell tracking experiments. It is important to mention that the total amount of iron oxides administrated *in vivo* corresponded to 5 μg of iron per mouse, which is low compared with total body iron. In our cell tracking experiments, it was therefore not possible to measure degraded forms of SPIOs and thus to investigate SPIO metabolism after injection. Our observations are in line with the study of Levy *et al.* (15), who investigated SPIO metabolism *in vivo* and showed that inductively coupled plasma optical emission spectrometry did not allow detection of exogenous iron oxides in tissues when low doses of SPIOs were injected. In a recent study, it was shown using histology that the number of 4 T1 cells in the brain decreased with time over 3 days following intracardiac injection (33). These data suggest that removal of dead cells plays a major role in the observed loss of negative contrast in the present *in vivo* MR images. However, the use of reporter gene-based methods such as BLI allows repetitive imaging for extended periods compared with cell tracking methods using intracellular contrast agents.

Interestingly, we found that MIRB-labeled cancer cells survived in the brain and led to the formation of micrometastases (~100 μm). We were not able to observe these brain micrometastases *in vivo* using MRI. However, using BLI we visualized metastases that developed in the lungs and in the bones after intracardiac injection of 4 T1-luc cells. These results are consistent with our EPR data showing that SPIO-labeled CTCs are entrapped in the lungs 4 h after injection.

Although other studies have reported the use of MRI cell tracking to study brain metastasis formation after the intracardiac injection of cancer cells (30,34,35), in this work we report for the first time the quantification of SPIOs in the mouse brain after administration of murine breast cancer cells labeled with SPIOs. Using EPR, we calculated that ~8000 (<1%) of the injected cells (10^6) were found in the brain 4 h after intracardiac injection

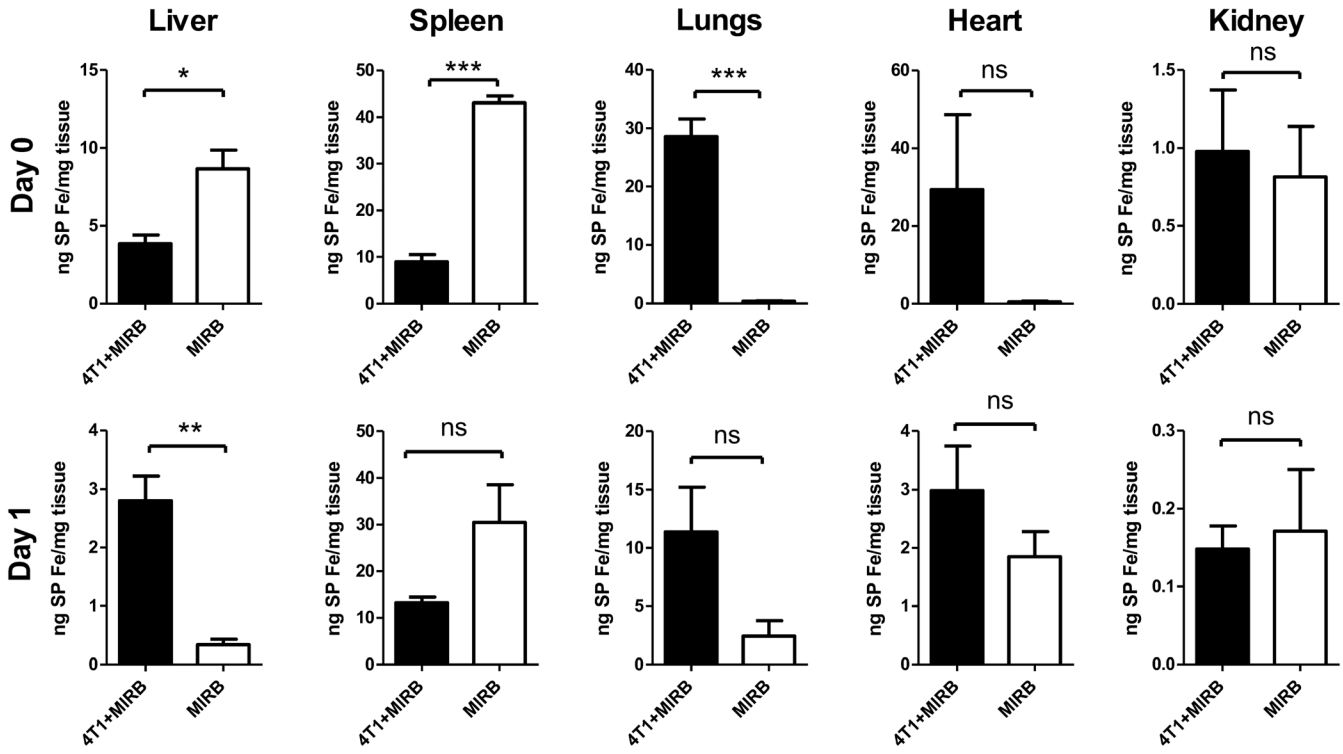

Figure 6. Biodistribution of iron oxides after intracardiac injection of MIRB-labeled 4 T1-luc cells or free MIRB nanoparticles. SPIO levels were quantified using *ex vivo* EPR in organs of mice injected with 10^6 MIRB-labeled cells or 5 μg SP Fe of free MIRB particles. 4 h post-injection (day 0), higher SPIO amounts were found in the liver and the spleen of mice injected with free MIRB particles ($n = 3$). On the other hand, lungs of mice injected with MIRB-labeled 4 T1-luc cells contained significantly higher levels of iron oxides 4 h after injection compared with mice injected with free MIRB ($n = 3$). A decrease in SPIO levels was observed in organs of both groups one day post-injection ($n = 4$). Data are expressed as mean ± SEM. $^*p < 0.05$, $^{**}p < 0.01$, $^{***}p < 0.001$, ns, $p > 0.05$.

(dry weight of the brain ~ 80 mg, injection of 10^6 MIRB-labeled 4 T1 cells containing 5 pg Fe, ~500 pg Fe/mg brain tissue 4 h after injection). Considering that blood flow to the mouse brain represents only 3% of the cardiac output (36), our results indicate that one quarter of the CTCs in the brain were entrapped 4 h after injection. These calculations assume that cells did not start to proliferate after injection (4 h). At later time points, cells would start to divide and the intracellular iron oxide content would be shared among daughter cells (27). Hence, an estimation of the number of iron oxide-labeled cells in tissues using *ex vivo* EPR is only valid shortly after cell delivery.

MRI was shown to precisely localize labeled cancer cells in the brain, but the number of hypointense spots did not necessarily correspond to the number of cells. As shown with Prussian blue staining, signal voids on gradient-echo images could be due to isolated but also to small clusters of SPIO-labeled cells. Their visualization on T_2*-w images is also limited by artifacts due to air–tissue interfaces (ears, oral cavity).

Although the dilution of intracellular iron oxides with cell division and uptake of free SPIO by macrophages limits the monitorable period of labeled cells in MRI cell tracking studies, the ability to visualize and quantify CTCs using magnetic cell tracking approaches has still a great potential for studying cancer metastases (27,37). To our knowledge we are the first to provide a straightforward estimation of SPIO-labeled CTCs in the mouse brain. This will be helpful for understanding early steps of the metastatic cascade, including the survival in the blood stream, extravasation and micrometastasis formation.

In a previous study, Heyn *et al*. showed using another breast cancer brain metastasis model (intracardiac injection of MDA-MB231BR human breast cancer cells) that a subset of SPIO-labeled cancer cells (visible using MRI) formed large metastases (hyperintense lesions on MRI scans) (34). The authors were thus able to assess the fate of CTCs in the brain and to determine whether isolated cancer cells were proliferating (macrometastasis formation), quiescent (contrast persistence on MR images) or transiently present in the brain tissues (quick loss of contrast). Using a similar approach with a liver metastasis model, Townson *et al*. showed that the chemotherapeutic agent doxorubicin reduced the size of liver metastases but not the overall number of solitary dormant cells in the liver (visualized thanks to MRI cell tracking) (38). These two studies highlighted the potential role of MRI cell tracking for elucidating tumor dormancy mechanisms and characterizing the efficacy of anticancer drugs on metastatic progression. In contrast to the study by Heyn *et al*., we did not observe any brain macrometastases development after injection of 4 T1-luc cells. This can be explained by the fact that 4 T1-luc cells may have a lower tropism for the brain compared with 'brain seeking' tumor models such as MDA-MB231BR cells. Another difference is that 4 T1-luc murine cancer cells rapidly grew *in vivo* compared with MDA-MB231BR human cancer cells. This explained why the longitudinal monitoring of mice could not exceed 13 days. Mice were indeed showing signs of weakness due to systemic cancer progression.

In conclusion, *ex vivo* EPR and MRI are complementary methods for cell tracking applications, even though in our study a correct estimate of the number of labeled cells using

NMR IN BIOMEDICINE

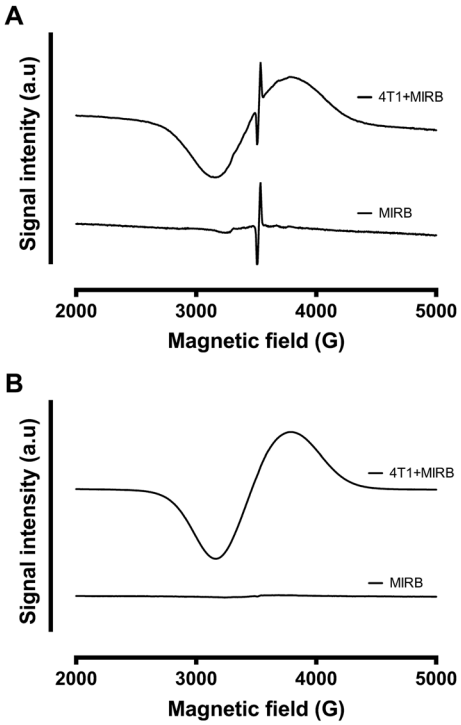

Figure 7. Representative EPR spectra of brain (A) and lung (B) tissues recorded *ex vivo* 4 h after intracardiac injection of MIRB-labeled 4 T1-luc cells or free MIRB. A broad EPR spectrum corresponding to iron oxides was observed in brains (A) and lungs (B) of mice injected with MIRB-labeled 4 T1-luc, whereas no EPR signal was detected in these organs in mice injected with free nanoparticles. *Y*-axis scales were adapted for presentation purposes.

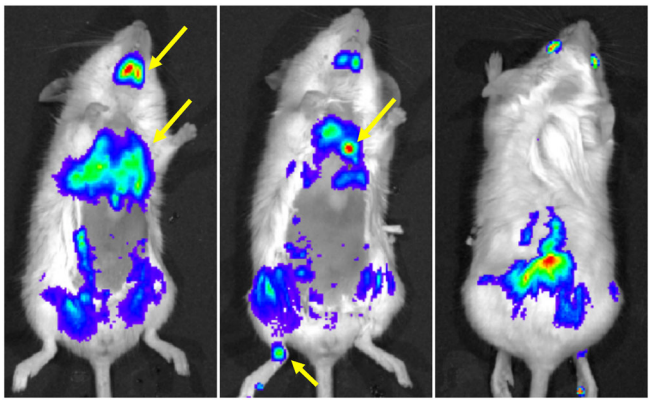

Figure 8. Representative BLI pictures of mice 6 days following intracardiac injection of 4 T1-luc cells. BLI showed that this cell line preferentially metastasized to the lungs and joints (yellow arrows). BLI positive spots were also detected at the injection site (heart). Of note, no photons arising from 4 T1-luc cells in the brain could be detected.

EPR was possible only within a few hours after cell injection. Owing to the highly proliferative phenotype of cancer cells, the iron oxide content per cell is decreased over time following administration. Of importance, besides cancer, cell-based therapies using cells with lower proliferative potential constitute a main field of applications for MRI cell tracking (39). For such studies, EPR could be complementary to MRI in assessing the biodistribution of SPIO-labeled cells for prolonged periods of time after administration.

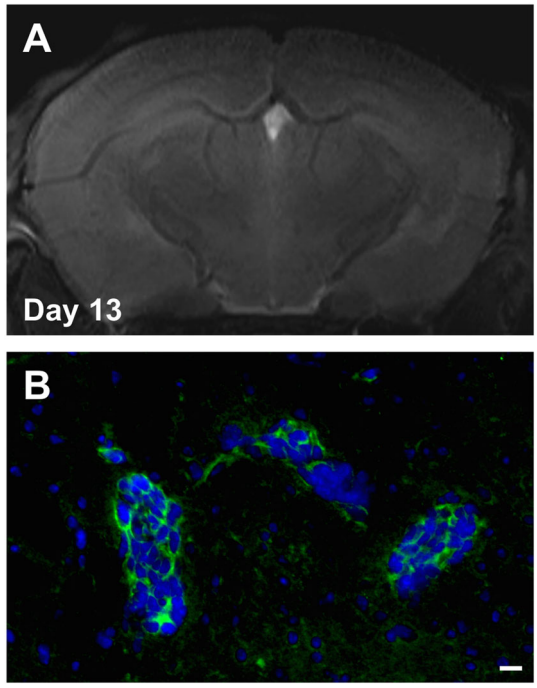

Figure 9. Long-term assessment of the presence of 4 T1-luc cells in mouse brains following intracardiac administration. No macrometastases could be detected using anatomical T_2-w images (A) ($n = 3$), whereas immunofluorescence studies (B) demonstrated the presence of 4 T1-luc micrometastases 13 days after injection of 10^6 4 T1-luc cells ($n = 3$). Luciferase-positive cells are stained in green and nuclei are stained in blue using Hoechst 33342. The scale bar represents 20 μm.

SUPPLEMENTARY MATERIAL

Cell labeling

Luciferase-expressing 4 T1-luc murine breast cancer cells were grown in Dulbecco's modified Eagle medium + GlutaMAX (Invitrogen, Merelbeke, Belgium), supplemented with 10% (v/v) fetal bovine serum (Invitrogen) and 1% (v/v) penicillin/streptomycin (Invitrogen). Two days before experiment, 10^4 cells/cm^2 were seeded in plastic dishes. The next day, they were incubated overnight with 20 μg Fe/mL MIRB particles (BioPAL, Worcester, MA, USA) in full medium. After labeling, cells were washed three times with phosphate-buffered saline (PBS), trypsinized, centrifuged and resuspended in PBS. Cells were then counted using a hemocytometer and viability was assessed using Trypan blue dye; they were centrifuged again and kept on ice in a PBS solution. They were injected into animals within 30 min after preparation.

Intracellular iron oxide content quantification and SPIO localization after labeling

Intracellular iron oxide content per cell was determined using EPR as previously described (18). Fluorescence microscopy was performed to assess the cellular localization of red fluorescent MIRB nanoparticles after labeling. Briefly, cells were seeded on Lab-Tek chamber slides (Sigma-Aldrich, Diegem, Belgium) and incubated overnight in full medium with MIRB particles (20 μg Fe/mL). Cells

were rinsed three times with PBS, fixed with paraformaldehyde 4% (Sigma) and permeabilized with PBS/0.1% Triton. Actin was stained using phalloidin-FITC (Sigma). Slides were then mounted using VECTASHIELD (Vector Labs, Brussels, Belgium), and images were captured on a Zeiss Axio Imager fluorescence microscope equipped with an ApoTome module (structured illumination).

Intracardiac injection of 4 T1-luc cells

Five-week-old female BALB/c mice (Janvier, Le Genest-Saint-Isle, France) were anesthetized with ketamine (80 mg/kg)/xylazine (8 mg/kg). 100 μL of PBS containing MIRB-labeled 4 T1-luc cells or free MIRB particles were then slowly injected into the left ventricle using an insulin syringe.

SPIO detection in the mouse brain using Prussian blue staining

Four hours after intracardiac injection of MIRB-labeled 4 T1-luc cells (2×10^6 cells), *in vivo* MRI was performed to detect labeled cells in the brain. Mice with SPIO-LABELED cells detected in the brain were sacrificed and the brains were collected. After overnight fixation at 4 °C in 4% paraformaldehyde, brains were embedded in paraffin and 5 μm coronal sections were made. Iron oxide presence was revealed using Prussian blue staining and slides were counterstained with periodic acid–Schiff.

Bioluminescence imaging

Bioluminescence imaging (BLI) was performed on mice 6 days after injection of 10^6 4 T1-luc cells. Mice were anaesthetized with ketamine (80 mg/kg)/xylazine (8 mg/kg) and depilated. Luciferin (150 mg/kg) was injected intraperitoneally and BLI images were acquired 15 min after injection using an IVIS50 imaging system (Xenogen) and a 16-bit digitizer.

Histological detection of 4 T1-luc brain metastases

To assess the presence of 4 T1-luc brain micrometastases in mice that were repetitively scanned using MRI, mice were sacrificed 13 days post-injection and the brains were embedded in optimum cutting temperature compound (Gentaur, Kampenhout, Belgium) and frozen with liquid nitrogen vapor; 10 μm coronal sections were made using a cryostat. Sections were fixed for 10 min in cold acetone. After blocking, sections were incubated with a rabbit anti-luciferase antibody (Abcam, Cambridge, UK). Luciferase-expressing cells were revealed with an Alexa 488 mouse anti-rabbit secondary antibody (Invitrogen). Nuclei were stained using Hoechst 33342 (Sigma).

Acknowledgements

We thank Rose-Marie Goebbels and Chantal Fregimilicka for histology. This work was supported by grants from the Fonds National de la Recherche Scientifique (FRS-FNRS), the Fonds Joseph Maisin, the Saint-Luc Foundation, the 'Actions de Recherches Concertées–Communauté française de Belgique – ARC 09/14-020', the European Research Council (FP7/2007–2013 ERC Independent Researcher Starting Grant No 243188 TUMETABO to P. Sonveaux), the Belgian Fondation contre le Cancer, and Interuniversity Attraction Pole (IAP) Grant No UP7-03 from the Belgian Science Policy Office (BELSPO). Funders had no role in study design, data collection and analysis, decision to publish, or preparation of the manuscript. B. F. Jordan and P. Sonveaux are Research Associates, P. E. Porporato is a Postdoctoral Researcher and P. Danhier is a Research Fellow of the FRS-FNRS. G. De Preter is a Télévie Research Fellow. The authors have declared that no competing interests exist.

REFERENCES

1. Kircher MF, Gambhir SS, Grimm J. Noninvasive cell-tracking methods. Nat. Rev. Clin. Oncol. 2011; 8(11): 677–688.
2. Cohen B, Dafni H, Meir G, Harmelin A, Neeman M. Ferritin as an endogenous MRI reporter for noninvasive imaging of gene expression in C6 glioma tumors. Neoplasia 2005; 7(2): 109–117.
3. Iordanova B, Ahrens ET. *In vivo* magnetic resonance imaging of ferritin-based reporter visualizes native neuroblast migration. Neuroimage 2012; 59(2): 1004–1012.
4. Vande Velde G, Raman Rangarajan J, Vreys R, Guglielmetti C, Dresselaers T, Verhoye M, Van der Linden A, Debyser Z, Baekelandt V, Maes F, Himmelreich U. Quantitative evaluation of MRI-based tracking of ferritin-labeled endogenous neural stem cell progeny in rodent brain. Neuroimage 2012; 62(1): 367–380.
5. Bulte JW, Kraitchman DL. Iron oxide MR contrast agents for molecular and cellular imaging. NMR Biomed.. 2004; 17(7): 484–499.
6. Smirnov P, Gazeau F, Beloeil JC, Doan BT, Wilhelm C, Gillet B. Single-cell detection by gradient echo 9.4 T MRI: a parametric study. Contrast Media Mol. Imaging 2006; 1(4): 165–174.
7. Foster-Gareau P, Heyn C, Alejski A, Rutt BK. Imaging single mammalian cells with a 1.5 T clinical MRI scanner. Magn. Reson. Med. 2003; 49(5): 968–971.
8. Langley J, Liu W, Jordan EK, Frank JA, Zhao Q. Quantification of SPIO nanoparticles in vivo using the finite perturber method. Magn. Reson. Med. 2011; 65(5): 1461–1469.
9. Kotek G, van Tiel ST, Wielopolski PA, Houston GC, Krestin GP, Bernsen MR. Cell quantification: evolution of compartmentalization and distribution of iron-oxide particles and labeled cells. Contrast Media Mol. Imaging 2012; 7(2): 195–203.
10. Girard OM, Ramirez R, McCarty S, Mattrey RF. Toward absolute quantification of iron oxide nanoparticles as well as cell internalized fraction using multiparametric MRI. Contrast Media Mol. Imaging 2012; 7(4): 411–417.
11. Rad AM, Arbab AS, Iskander AS, Jiang Q, Soltanian-Zadeh H. Quantification of superparamagnetic iron oxide (SPIO)-labeled cells using MRI. J. Magn. Reson. Imaging 2007; 26(2): 366–374.
12. Liu W, Frank JA. Detection and quantification of magnetically labeled cells by cellular MRI. Eur. J. Radiol.. 2009; 70(2): 258–264.
13. van Buul GM, Kotek G, Wielopolski PA, Farrell E, Bos PK, Weinans H, Grohnert AU, Jahr H, Verhaar JA, Krestin GP, van Osch GJ, Bernsen MR. Clinically translatable cell tracking and quantification by MRI in cartilage repair using superparamagnetic iron oxides. PLoS One 2011; 6(2): e17001.
14. Chertok B, Cole AJ, David AE, Yang VC. Comparison of electron spin resonance spectroscopy and inductively-coupled plasma optical emission spectroscopy for biodistribution analysis of iron-oxide nanoparticles. Mol. Pharm. 2010; 7(2): 375–385.
15. Levy M, Luciani N, Alloyeau D, Elgrabli D, Deveaux V, Pechoux C, Chat S, Wang G, Vats N, Gendron F, Factor C, Lotersztajn S, Luciani A, Wilhelm C, Gazeau F. Long term in vivo biotransformation of iron oxide nanoparticles. Biomaterials 2011; 32(16): 3988–3999.
16. Serres S, Soto MS, Hamilton A, McAteer MA, Carbonell WS, Robson MD, Ansorge O, Khrapitchev A, Bristow C, Balathasan L, Weissensteiner T, Anthony DC, Choudhury RP, Muschel RJ, Sibson NR. Molecular MRI enables early and sensitive detection of brain metastases. Proc. Natl. Acad. Sci. U. S. A. 2012; 109(17): 6674–6679.
17. Carbonell WS, Ansorge O, Sibson N, Muschel R. The vascular basement membrane as 'soil' in brain metastasis. PLoS One 2009; 4(6): e5857.
18. Danhier P, De Preter G, Boutry S, Mahieu I, Leveque P, Magat J, Haufroid V, Sonveaux P, Bouzin C, Feron O, Muller RN, Jordan BF, Gallez B. Electron paramagnetic resonance as a sensitive tool to assess the iron oxide content in cells for MRI cell labeling studies. Contrast Media Mol. Imaging 2012; 7(3): 302–307.

19. McFadden C, Mallett CL, Foster PJ. Labeling of multiple cell lines using a new iron oxide agent for cell tracking by MRI. Contrast Media Mol. Imaging 2011; 6(6): 514–522.
20. Radermacher KA, Beghein N, Boutry S, Laurent S, Vander Elst L, Muller RN, Jordan BF, Gallez B. In vivo detection of inflammation using pegylated iron oxide particles targeted at E-selectin: a multimodal approach using MR imaging and EPR spectroscopy. Invest. Radiol. 2009; 44(7): 398–404.
21. Radermacher KA, Boutry S, Laurent S, Elst LV, Mahieu I, Bouzin C, Magat J, Gregoire V, Feron O, Muller RN, Jordan BF, Gallez B. Iron oxide particles covered with hexapeptides targeted at phosphatidylserine as MR biomarkers of tumor cell death. Contrast Media Mol. Imaging 2010; 5(5): 258–267.
22. Radermacher KA, Magat J, Bouzin C, Laurent S, Dresselaers T, Himmelreich U, Boutry S, Mahieu I, Vander Elst L, Feron O, Muller RN, Jordan BF, Gallez B. Multimodal assessment of early tumor response to chemotherapy: comparison between diffusion-weighted MRI, ^{1}H-MR spectroscopy of choline and USPIO particles targeted at cell death. NMR Biomed.. 2012; 25(4): 514–522.
23. Iannone A, Federico M, Tomasi A, Magin RL, Casasco A, Calligaro A, Vannini V. Detection and quantitation in rat tissues of the superparamagnetic magnetic resonance contrast agent dextran magnetite as demonstrated by electron spin resonance spectroscopy. Invest. Radiol. 1992; 27(6): 450–455.
24. Danhier P, De Preter G, Magat J, Godechal Q, Porporato PE, Jordan BF, Feron O, Sonveaux P, Gallez B. Multimodal cell tracking of a spontaneous metastasis model: comparison between MRI, electron paramagnetic resonance and bioluminescence. Contrast Media Mol. Imaging 2014; 9(2): 143–153.
25. Sykova E, Jendelova P, Herynek V. Magnetic resonance imaging of stem cell migration. Methods Mol. Biol. 2011; 750: 79–90.
26. Slawska-Waniewska A, Mosiniewicz-Szablewsaka E, Nedelko N, Galazka-Friedman J, Friedman A. Magnetic studies of iron entities in human tissues. J. Magn. Magn. Mater. 2004; 272–276: 2417–2419.
27. Walczak P, Kedziorek DA, Gilad AA, Barnett BP, Bulte JW. Applicability and limitations of MR tracking of neural stem cells with asymmetric cell division and rapid turnover: the case of the shiverer dysmyelinated mouse brain. Magn. Reson. Med. 2007; 58(2): 261–269.
28. Weissleder R, Stark DD, Engelstad BL, Bacon BR, Compton CC, White DL, Jacobs P, Lewis J. Superparamagnetic iron oxide: pharmacokinetics and toxicity. Am. J. Roentgenol. 1989; 152(1): 167–173.
29. Arbab AS, Wilson LB, Ashari P, Jordan EK, Lewis BK, Frank JA. A model of lysosomal metabolism of dextran coated superparamagnetic iron oxide (SPIO) nanoparticles: implications for cellular magnetic resonance imaging. NMR Biomed. 2005; 18(6): 383–389.
30. Song HT, Jordan EK, Lewis BK, Liu W, Ganjei J, Klaunberg B, Despres D, Palmieri D, Frank JA. Rat model of metastatic breast cancer monitored by MRI at 3 tesla and bioluminescence imaging with histological correlation. J. Transl. Med. 2009; 7: 88.
31. Addicott B, Willman M, Rodriguez J, Padgett K, Han D, Berman D, Hare JM, Kenyon NS. Mesenchymal stem cell labeling and *in vitro* MR characterization at 1.5 T of new SPIO contrast agent: Molday ION Rhodamine-B^{TM}. Contrast Media Mol. Imaging 2011; 6(1): 7–18.
32. Shen WB, Plachez C, Chan A, Yarnell D, Puche AC, Fishman PS, Yarowsky P. Human neural progenitor cells retain viability, phenotype, proliferation, and lineage differentiation when labeled with a novel iron oxide nanoparticle, Molday ION Rhodamine B. Int. J. Nanomedicine 2013; 8: 4593–4600.
33. Balathasan L, Beech JS, Muschel RJ. Ultrasonography-guided intracardiac injection: an improvement for quantitative brain colonization assays. Am. J. Pathol. 2013; 183(1): 26–34.
34. Heyn C, Ronald JA, Ramadan SS, Snir JA, Barry AM, MacKenzie LT, Mikulis DJ, Palmieri D, Bronder JL, Steeg PS, Yoneda T, MacDonald IC, Chambers AF, Rutt BK, Foster PJ. In vivo MRI of cancer cell fate at the single-cell level in a mouse model of breast cancer metastasis to the brain. Magn. Reson. Med. 2006; 56(5): 1001–1010.
35. Perera M, Ribot EJ, Percy DB, McFadden C, Simedrea C, Palmieri D, Chambers AF, Foster PJ. *In vivo* magnetic resonance imaging for investigating the development and distribution of experimental brain metastases due to breast cancer. Transl. Oncol. 2012; 5(3): 217–225.
36. Barbee RW, Perry BD, Re RN, Murgo JP. Microsphere and dilution techniques for the determination of blood flows and volumes in conscious mice. Am. J. Physiol. 1992; 263(3 Pt 2): R728–733.
37. Terrovitis J, Stuber M, Youssef A, Preece S, Leppo M, Kizana E, Schar M, Gerstenblith G, Weiss RG, Marban E, Abraham MR. Magnetic resonance imaging overestimates ferumoxide-labeled stem cell survival after transplantation in the heart. Circulation 2008; 117(12): 1555–1562.
38. Townson JL, Ramadan SS, Simedrea C, Rutt BK, MacDonald IC, Foster PJ, Chambers AF. Three-dimensional imaging and quantification of both solitary cells and metastases in whole mouse liver by magnetic resonance imaging. Cancer Res.. 2009; 69(21): 8326–8331.
39. Cromer Berman SM, Walczak P, Bulte JW. Tracking stem cells using magnetic nanoparticles. Wiley Interdiscip. Rev. Nanomed. Nanobiotechnol. 2011; 3(4): 343–355.